AGU PUBLICATIONS

Geophysical Research Letters

RESEARCH LETTER
10.1002/2016GL067759

Key Points:
- In 2013 ice mass trends on and around Greenland diverged significantly from the long-term average
- The positive mass deviation over Greenland reached nearly 500 Gt by 2015
- Greenland and Canadian ice mass losses continue to accelerate while Alaskan loss has remained steady

Correspondence to:
C. Harig,
charig@princeton.edu

Citation:
Harig, C., and F. J. Simons (2016), Ice mass loss in Greenland, the Gulf of Alaska, and the Canadian Archipelago: Seasonal cycles and decadal trends, *Geophys. Res. Lett.*, *43*, 3150–3159, doi:10.1002/2016GL067759.

Received 13 JAN 2016
Accepted 5 MAR 2016
Accepted article online 10 MAR 2016
Published online 5 APR 2016

Ice mass loss in Greenland, the Gulf of Alaska, and the Canadian Archipelago: Seasonal cycles and decadal trends

Christopher Harig[1] and Frederik J. Simons[1]

[1]Department of Geosciences, Princeton University, Princeton, New Jersey, USA

Abstract Over the past several decades mountain glaciers and ice caps have been significant contributors to sea level rise. Here we estimate the ice mass changes in the Canadian Archipelago, the Gulf of Alaska, and Greenland since 2003 by analyzing time-varying gravimetry data from the Gravity Recovery and Climate Experiment. Prior to 2013, interannual ice mass variability in the Gulf of Alaska and in regions around Greenland remains within the average estimated over the whole data span. Beginning in summer 2013, ice mass in regions around Greenland departs positively from its long-term trend. Over Greenland this anomaly reached almost 500 Gt through the end of 2014. Overall, long-term ice mass loss from Greenland and the Canadian Archipelago continues to accelerate, while losses around the Gulf of Alaska region continue but remain steady with no significant acceleration.

1. Introduction

Since 1990, the second largest contributor (behind thermal expansion) to global mean sea level rise has been the melting of mountain glaciers and ice caps, which have together shed more ice mass than the land ice sheets on Greenland and Antarctica [*Stocker et al.*, 2013]. Among these glaciers, the ones in the Canadian Archipelago and the Gulf of Alaska have experienced some of the largest estimated mass changes in the past decade [*Gardner et al.*, 2011; *Jacob et al.*, 2012]. Future projections of 21st century sea level rise depend on the quantity and location of land ice mass changes [e.g., *Bamber and Riva*, 2010; *Little et al.*, 2013a, 2013b], which require long-term continuous measurement to determine with high accuracy [*Wouters et al.*, 2013]. Earth's time-variable gravity field, as observed since 2002 by the Gravity Recovery and Climate Experiment (GRACE), has provided a highly detailed record of land ice mass change over the past decade [e.g., *Luthcke et al.*, 2008; *Velicogna*, 2009; *Chen et al.*, 2011; *King et al.*, 2012; *Harig and Simons*, 2015]. From the orbits and the range (rates) between twin satellites [*Tapley et al.*, 2004], a global gravity field is determined each month, or more frequently [*Luthcke et al.*, 2013]. Changes in the geopotential resolve the surface density to within centimeters of water equivalent (cm w.e.) [*Swenson et al.*, 2003].

Laser altimetry and GRACE gravimetry have both been used to determine the past ice mass loss rate of the Gulf of Alaska. Recent studies estimate mass loss (in gigatons per year) ranging from −61 Gt/yr to −75 Gt/yr [*Arendt et al.*, 2013; *Luthcke et al.*, 2013; *Sasgen et al.*, 2012]. While the overall trends show little or no acceleration, the region displays large interannual variations in mass, linked in some cases to climatic events [e.g., *Arendt et al.*, 2013]. Observations in the Canadian Archipelago indicate that ice mass loss acceleration during the 2000s [*Gardner et al.*, 2011, 2013; *Jacob et al.*, 2012] increased the rate of mass loss compared to twentieth century values [*Abdalati et al.*, 2004; *Gardner et al.*, 2012]. Recent estimates agree that from 2003 to 2010 mass loss rates have risen to roughly −30 Gt/yr for each of the northern and southern regions of the Canadian Archipelago. Continued long-term monitoring is needed, however, to determine if these accelerations fall within the variance of interannual variations, which can significantly impact the estimated ice mass loss rate [*Wouters et al.*, 2013].

Studying the cryosphere from GRACE data products requires "localization." We have a bandlimited global field on the sphere and wish to estimate its behavior over a specific geographic location, such as over an ice sheet. To this end, we use a modern spherical analogue [*Simons et al.*, 2006] of a classic signal processing technique [*Slepian*, 1983]. The spherical Slepian functions at the basis of our method are designed to minimize the "leakage" of the signal out of the region of interest [*Simons and Dahlen*, 2006]. Our method has previously

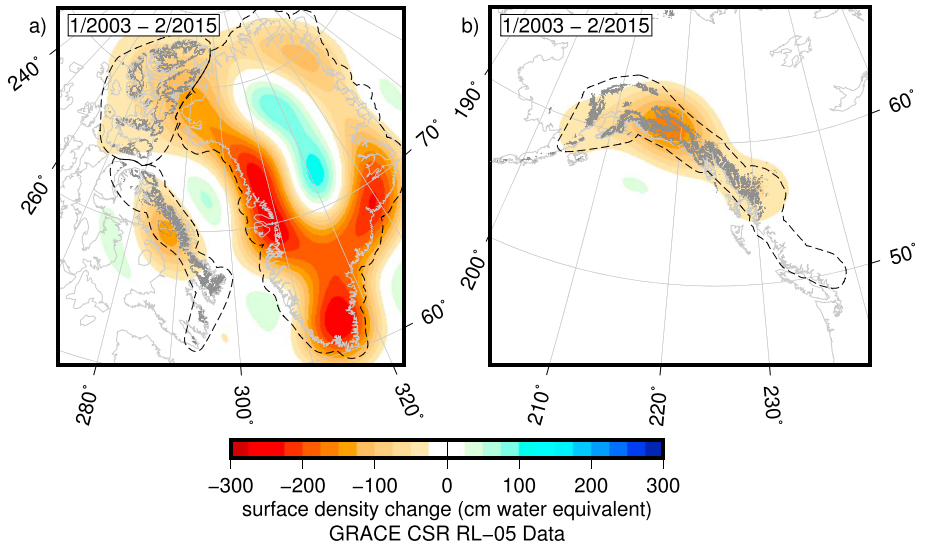

Figure 1. Map of the total ice mass change (mass corrected using the glacial isostatic adjustment (GIA) model by *Paulson et al.* [2007]) for the regions (black dashed lines) around (a) Greenland and (b) Gulf of Alaska. Coastlines are shown in light grey. Glaciated regions, as determined from the Randolph Glacier Inventory (RGI) version 3.2, are outlined in dark grey.

been applied to estimate the mass changes of Earth's large ice sheets [*Harig and Simons*, 2012, 2015]; however, the small regions considered here approach the resolution limit for its applicability using GRACE, and the various findings reported here constitute new evidence of system variability that will be targets for detection and analysis by other, nongravimetric studies.

Here we investigate ice mass changes in and around the Gulf of Alaska, the Canadian Archipelago, and Greenland since 2003. Our results will be of methodological interest to the gravity community as well as to the cryosphere and climate policy communities from the perspective of sea level rise contributions.

2. Methods

We use Slepian functions to localize the time-variable gravity field from GRACE. We briefly review our technique in this section.

2.1. Theory

Geopotential fields are routinely distributed as "Stokes" coefficients expanding spherical-harmonic basis functions. These functions form an orthogonal basis on the sphere in which each function spreads its energy indiscriminately over the entire planet. To analyze the geopotential over ice sheets and glaciers, specifically, we must isolate those contributions from the global field and resolve them over our regions of interest. As before [*Harig and Simons*, 2012, 2015] we project the geopotential into an alternate basis set, the Slepian functions, whose energy, and thus, sensitivity to signal, for a given bandwidth L, is maximized within the specific regions of interest R and minimized over the rest of the sphere Ω.

The spherical Slepian basis functions maximize their energy within a closed geographical contour on the sphere (e.g., Figure 1). We are thus looking for new functions g that maximize the ratio

$$\lambda = \int_R g^2 \, \mathrm{d}\Omega \Big/ \int_\Omega g^2 \, \mathrm{d}\Omega. \tag{1}$$

The functions g that we seek are bandlimited (all of them to the same maximum degree L) linear combinations of spherical harmonics. Hence, as shown by *Simons et al.* [2006], their expansion coefficients are found as the eigenfunctions of a Gram matrix that expresses how nonorthogonal the spherical harmonics are on mere portions of the unit sphere. We form the matrix of cross products of spherical harmonics and integrate them over the region, as

$$\int_R Y_{lm} Y_{l'm'} \, \mathrm{d}\Omega = D_{lm,l'm'}. \tag{2}$$

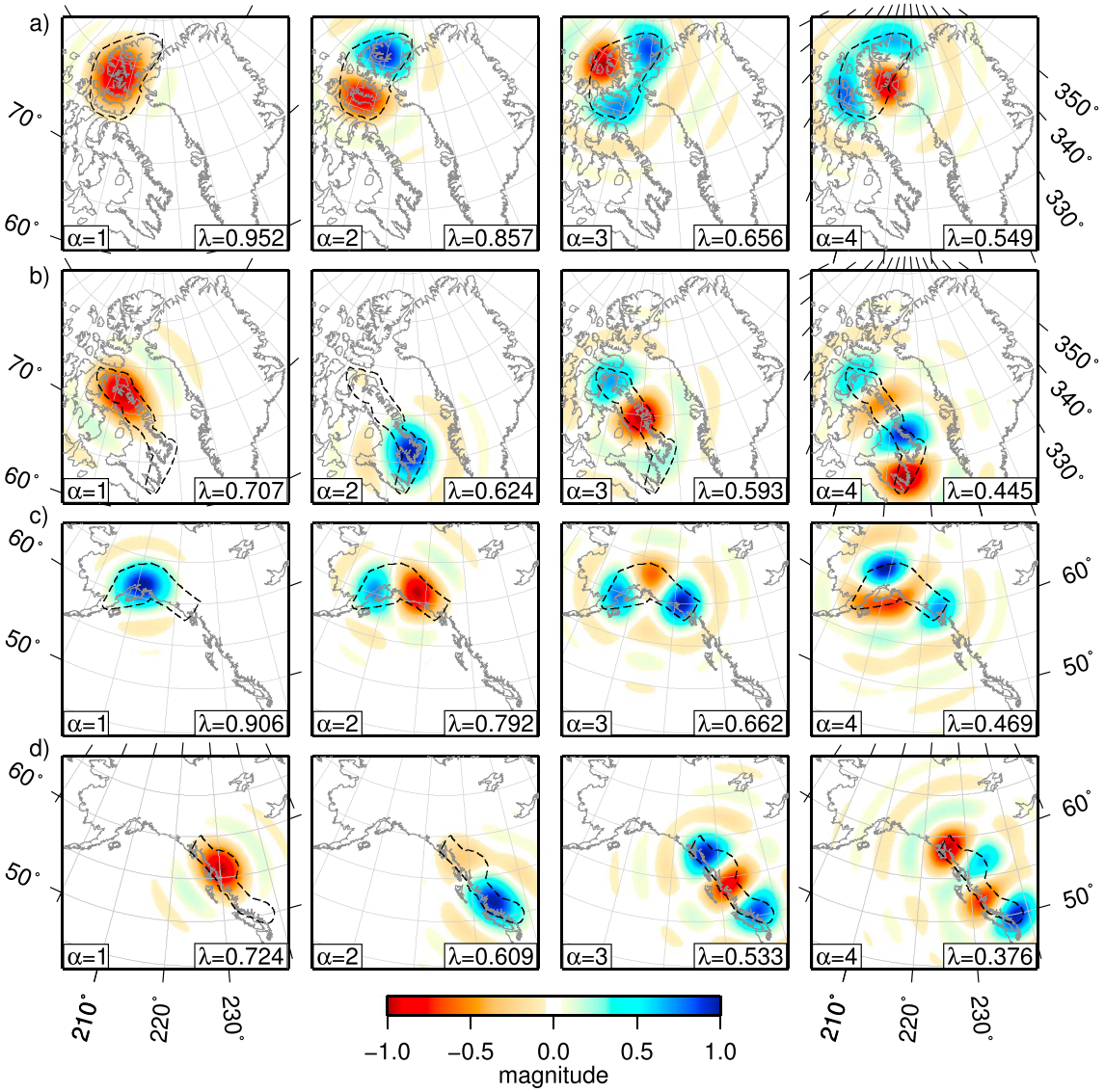

Figure 2. Slepian eigenfunctions that are optimally concentrated within regions (grouped by row) outlining (a) Ellesmere Island, (b) Baffin Island, (c) Gulf of Alaska North, and (d) Gulf of Alaska South. Dashed lines indicate the regions of concentration. Functions are bandlimited to $L = 60$ and are scaled to unit magnitude. The parameter α denotes which eigenfunction is shown. The parameter λ is the corresponding eigenvalue for each function, indicating the amount of concentration. Magnitude values whose absolute values are smaller than 0.01 are left white.

The Slepian functions (Figure 2) then result as the orthogonal eigenfunctions of the decomposition of this symmetric matrix,

$$\sum_{l'=0}^{L} \sum_{m'=-l'}^{l'} D_{lm,l'm'} g_{l'm'} = \lambda g_{lm}, \tag{3}$$

and the eigenvalues λ rank each function by its degree of concentration in the region. There are just as many Slepian functions, $(L+1)^2$, as there were elements in the bandlimited spherical-harmonic basis, but they are doubly orthogonal, over the sphere Ω and the region R, and the relatively few high-eigenvalue ($\lambda \gtrsim 0.5$) functions are an effectively truncated, approximate basis for bandlimited processes over the region. The entire set remains a complete basis for processes with the same bandwidth over the whole sphere.

In Figure 2 we show the first four optimally concentrated Slepian functions for four different regions. Due to their small area and the bandwidth used, only a few functions are well concentrated. Other Slepian functions have more energy outside of the region of interest. By selecting only the most concentrated Slepian functions,

we reduce the degrees of freedom of the estimation problem. For Greenland, which covers 0.5% of the Earth's surface, the number of parameters estimated via our method is just 0.5% of the number of spherical harmonics that would need to be estimated otherwise.

2.2. Practice

Three fundamental principles help us understand the estimation uncertainties. First, there is the global signal-to-noise ratio of the spherical-harmonic GRACE times series at the degrees approaching the bandwidth $L = 60$. This ratio depends on a multitude of processing details [e.g., *Flechtner et al.*, 2010], but overall the solutions are considered resolvable down to spatial scales of about 400 km over temporal scales of about 10 days [*Rowlands et al.*, 2005]. Second, there is the fundamental unit of information in spatiospectral localization analysis, the space-bandwidth product or "Shannon number," $N = \lfloor (L+1)^2 A/(4\pi) \rfloor$, with $A/(4\pi)$ the area of the region of interest expressed as a fraction of the entire globe. This is a fundamental mathematical property, not unlike the Heisenberg uncertainty principle in signal processing, whose bounds the best-concentrated Slepian functions achieve almost exactly [*Kennedy and Sadeghi*, 2013]. Third, there is the amount of increase in the signal-to-noise ratio that is achieved when a local signal is isolated from the global field by projecting the spherical-harmonic solutions onto the first N terms of the localized Slepian basis. This behavior depends on the properties of the signal itself. The theoretical foundations, statistical implications, and the practicalities of the Slepian methodology are very well understood [*Simons and Plattner*, 2015; *Plattner and Simons*, 2015], as indeed they are for various other methods of localization [e.g., *Wahr et al.*, 2006; *Schrama et al.*, 2007; *Klees et al.*, 2008; *Velicogna and Wahr*, 2013]. Nevertheless, it is hard to gain a realistic appreciation of the uncertainty of the end products of our analysis without synthetic recovery simulation experiments [e.g., *Velicogna and Wahr*, 2006; *Harig and Simons*, 2012], which we conducted along the same lines in this paper.

2.3. Application

We used 135 months (January 2003 to February 2015) of GRACE RL-05 data from the Center for Space Research at University of Texas at Austin, distributed as monthly global spherical-harmonic coefficients, but use degree 2 order 0 coefficients from satellite laser ranging [*Cheng et al.*, 2013]. The degree 1 coefficients for geocenter motion are calculated from *Swenson et al.* [2008]. We transform the geopotential into surface mass density, accounting for elastic deformation of the solid Earth resulting from surface mass changes using the load Love numbers of *Wahr et al.* [1998]. We regard as negligible the gravitational effects of local sea level retreat accompanying (ice) mass loss [*Sterenborg et al.*, 2013]. Although the specific degree 1 and degree 2 coefficients, and Love numbers may vary somewhat between research groups, our preliminary steps conform to standard practice in the GRACE community [see, e.g., *Reager et al.*, 2016, supporting information section S1].

We subtract a model for glacial isostatic adjustment (GIA) from *Paulson et al.* [2007] to remove the viscous solid-Earth response to previous deglaciation. Such corrections are definitely uncertain [e.g., *Guo et al.*, 2012], but their size provides some measure of guidance as to their influence on our final results, whose error bars do not include the GIA correction uncertainty per se. For Greenland, the correction is on the order of 5.4 Gt/yr; for Ellesmere, 6.7 Gt/yr; Baffin 3.6 Gt/yr; and for the Gulf of Alaska, 0.9 Gt/yr in the North and 1.9 Gt/yr in the South; all subtracted from the total mass signal to yield the contribution due to ice loss proper.

In areas outside of ice sheets, such as the Canadian Archipelago and the Gulf of Alaska, the gravity field is influenced by changes in water mass in the upper few meters of the Earth. To take those into account, we remove monthly estimates of terrestrial water storage (TWS) from the Global Land Data Assimilation System 1.0 (Noah), except in areas covered by glaciers, where they are known to be unreliable [*Arendt et al.*, 2013], again in keeping with GRACE community practice [see *Shepherd et al.*, 2012, supporting information section S8]. Here too these corrections have a some uncertainty, but their relative size is small: for the Gulf of Alaska (North), where they are most important, TWS effects oscillate between $\pm$10 Gt. In all areas TWS corrections are primarily seasonal and contribute virtually nothing to any of our quoted rate and acceleration estimates.

We use the Randolph Glacier Inventory [*Pfeffer et al.*, 2014] to outline broad glacial regions in the Canadian Archipelago and near the Gulf of Alaska for our localization. We used input/output simulations (as in *Harig and Simons* [2012, supporting information]) to determine the size of each region so as to best account for mass losses near the edges. The regions were slightly enlarged with a buffer of 0.5°, without overlap. For each buffered region we construct a Slepian basis which only depends on its outline and the bandwidth of the data, $L = 60$. The basis is truncated at the Shannon number, N. An effective metric of resolution, the Shannon numbers for the regions, can be found in Table 1.

Table 1. Ice Mass Trend Estimates (01/2003–05/2013) of the Various Regions in Gigatons per Year (Gt/yr)[a]

N	Region	Ice Mass Trend (Gt/yr)
20	Greenland (GR)	−244 ± 6
4	Ellesmere Region (EL)	−38 ± 2
3	Baffin Region (BA)	−22 ± 2
24	Greenland and Ellesmere Region	−274 ± 6
	Sum of two individual regions (GR + EL)	−282
27	Greenland, Ellesmere, and Baffin Islands	−304 ± 6
	Sum of three individual regions (GR + EL + BA)	−305
4	Gulf of Alaska, North	−36±4
3	Gulf of Alaska, South	−4±3

[a]The first column lists the Shannon number $N = (L + 1)^2(A/4\pi)$. The sums of the estimates made over individual regions are compared with estimates localized over the regions combined. They should closely agree, and they do.

GRACE fields for surface mass density are projected into each specific Slepian basis resulting in a time series for each coefficient. For each Slepian coefficient we fit a function to the time series, consisting of annual and semiannual periodic components, and up to a third-order polynomial, if the polynomial passes an *F* test for significance over the lower orders. We tested and rejected the need for a tidal aliasing (161 day) periodic term. We use a generalized least squares fit procedure which iteratively solves for the full covariance model of heteroscedasticity and autocorrelation in the presence of an AR(1) autoregressive noise process, as suggested by *Williams et al.* [2014], implemented using MATLAB's `fgls`. All of our uncertainties are presented at the 95% confidence ("2σ") level. We can multiply each estimate by the corresponding eigenfunction and expand these fits to physical space to form maps representing the long-term changes in surface density. Integration of these fields over the region results in the total mass change over time.

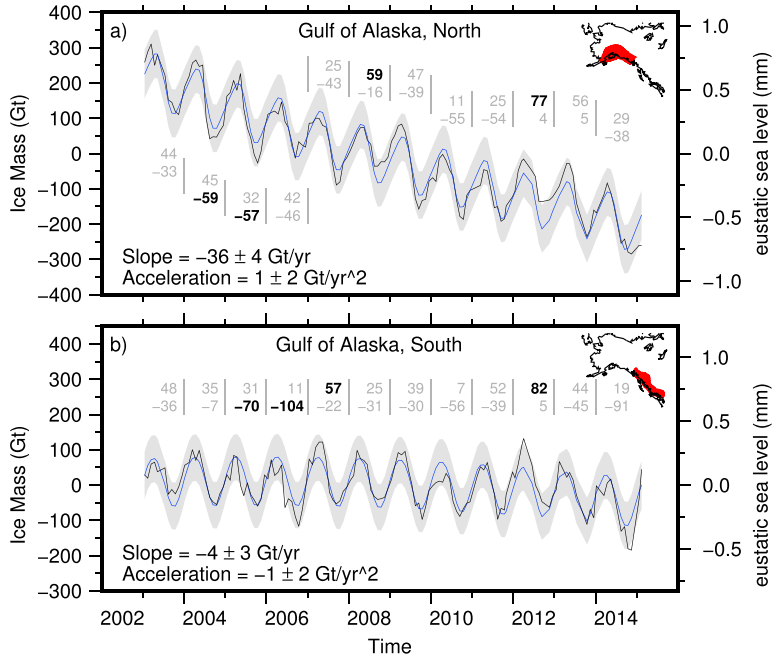

Figure 3. Ice mass changes (mass corrected using the GIA model by *Paulson et al.* [2007]) in gigatons (Gt) for (a) North and (b) South regions of the Gulf of Alaska. The regions covered by each localization are shaded red in the top right inset. The black lines are monthly GRACE observations with 2σ grey error bars determined from our analysis. The solid blue lines are the best fit estimates including a quadratic curve and the periodic annual and semiannual terms. For each year in the analysis, two numbers indicate the maximum (top) and minimum (bottom) difference between the observations and the fitted curves.

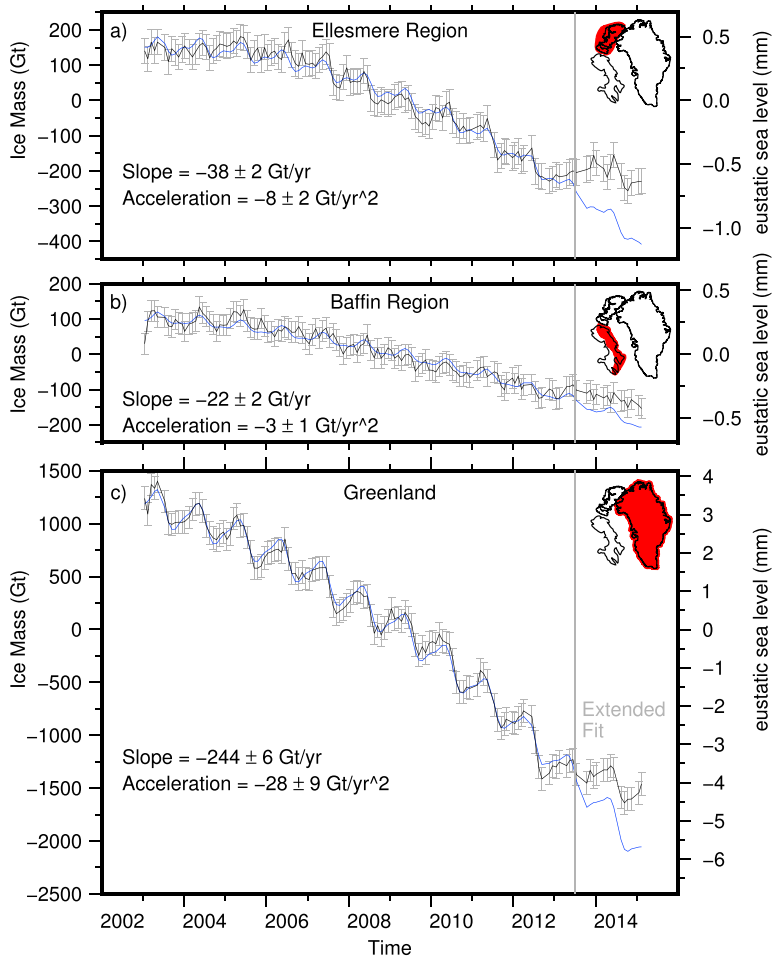

Figure 4. Ice mass changes (mass corrected using the GIA model by *Paulson et al.* [2007]) in gigatons (Gt) for regions of (a) Ellesmere Island, (b) Baffin Island, and (c) Greenland. The regions covered by each localization are shaded red in the top right inset. The black lines are monthly GRACE observations with 2σ grey error bars determined from our analysis. The solid blue lines are the best fit estimates including a quadratic curve and the periodic annual and semiannual terms. Estimates are fit using data prior to June 2013 (left of vertical grey lines) and then extrapolated forward through 2014 (right of vertical grey lines) to show the departure of recent data from the long-term trends.

3. Results

3.1. Alaska

We calculate the mass changes in two regions of the Gulf of Alaska. In the North region (Figure 3a) ice mass has been lost since 2003 at a rate of -36 ± 4 Gt/yr with an acceleration of 1 ± 2 Gt/yr^2. Fitting without considering the quadratic term results in trend estimates that are only different in the second decimal place. One of the distinguishing features of the mass trend in this area is the magnitude of annual variations, both in the estimated annual signal, and in departures of the data from the long-term average. During 2009, for example, the amount of ice lost during the summer melt season was above average, resulting in part from albedo changes on the glacier surfaces [*Arendt et al.*, 2013]. In the South region (Figure 3b), ice mass was lost in the past 12 years at a rate of -4 ± 3 Gt/yr with an acceleration of -1 ± 2 Gt/yr^2, or trend estimates that are only different in the first decimal place without fitting the acceleration.

3.2. The Canadian Archipelago

We examine two regions of the Canadian Archipelago, the Ellesmere Island region (northwest of Greenland), and the Baffin Island region (west of Greenland). Both of these have been losing ice mass since 2003 (Figures 4a and 4b). The integrated mass anomaly shows that Ellesmere Island was near mass balance in the first few years of the GRACE time series. By the end of 2008 (the midpoint of our estimation) the region was losing ice mass at a rate of -38 ± 2 Gt/yr with an acceleration of -8 ± 2 Gt/yr^2. The years 2011 and 2012 exhibited the

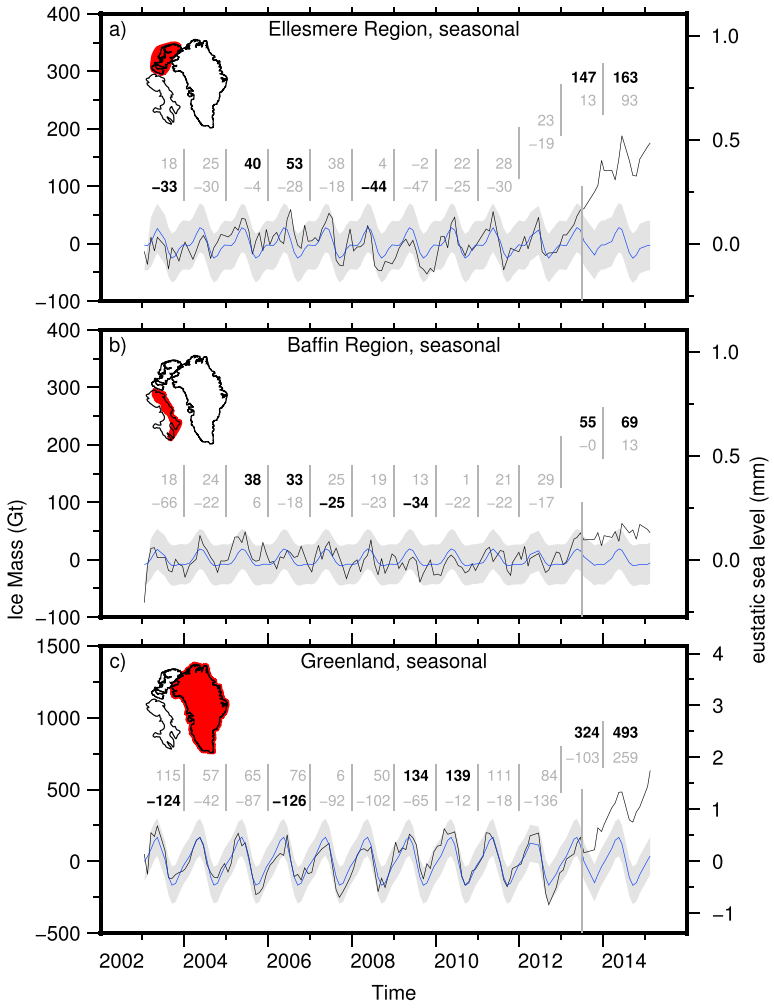

Figure 5. Ice mass changes found after removing the long-term trend and accelerations from the curves shown in Figure 4, leaving only the annual and semiannual components (blue lines) fitted from the data (black lines). The regions covered by each localization for of (a) Ellesmere Island, (b) Baffin Island, and (c) Greenland are shaded red in the inset. As in Figure 4, estimates are fit using data prior to June 2013 (left of vertical grey lines) and then extrapolated forward through 2014 (right of vertical grey lines) to show the departure of recent data from the long-term trends. The grey bands around the blue lines represent the 2σ confidence intervals for the prediction of new data points. Yearly numbers indicate the maximum (top) and minimum (bottom) difference between the observations and the fitted curves.

largest mass loss since 2003 in the Archipelago. Beginning in mid-2013 the mass anomaly starts to significantly diverge from the long-term decadal trends. To illustrate this point, we end our estimation with the data up to June 2013 and extend the fit forward to cover the rest of the time span (vertical grey lines in Figure 4). During the summer melt season of 2013, the mass of Ellesmere Island increased compared to several months prior, before decreasing again in 2014, causing a difference on the order of 150 Gt between the observations and the long-term decadal trend.

Baffin Island has also exhibited long-term mass loss since 2003, at a rate of -22 ± 2 Gt/yr with an acceleration of -3 ± 1 Gt/yr^2. Both values are lower than in Ellesmere Island. The mass for Baffin Island similarly diverges from its long-term trend during 2013, but at a smaller offset of about 50 Gt. Mass loss has been concentrated in the area of the Barnes Ice Cap (around latitude and longitude 70°, 286°), which has been losing mass for decades, at an increasing rate more recently [*Gardner et al.*, 2012].

The departure between the mass loss and the long-term trend in recent years becomes more clear when we remove the fitted long-term trend and acceleration from the time series and compare what remains to the fitted seasonal components (Figure 5a). Prior to 2013, interannual variations in the mass of Ellesmere Island are fairly well represented by an average seasonal cycle. The maximum (top row of grey values) and minimum

Table 2. Attributes of the Fitted Seasonal Ice Mass Cycles for Individual Regions[a]

Region	Seasonal Minimum (Gt)	Seasonal Maximum (Gt)	Seasonal per Unit Area (cm w.e.)
Ellesmere Region	−25	28	4.9
Baffin Region	−10	19	4.3
Greenland	−166	168	6.2
Gulf of Alaska, North	−81	76	15.0
Gulf of Alaska, South	−70	64	18.1

[a]We list the maximum and minimum values of the seasonal mass cycle, in gigatons (Gt). The larger of these in absolute value is used for the magnitude of the seasonal cycle per unit area of the region, quoted in cm water equivalent (cm w.e.).

(bottom row of grey values) differences between the data and seasonal cycle within each year are on the order of ±30 Gt. In 2013 and 2014 these differences reach upward of 150 Gt. Baffin Island displays similar variability to Ellesmere and shows a similar, but lower magnitude, departure from the trend since 2013 (Figure 5b). By 2014 the offset is roughly 75 Gt. We can compare these offsets to the magnitudes of the seasonal cycles in Table 2. The seasonal cycle in Baffin Island is 40–68% as large as the cycle in Ellesmere Island in absolute terms. When we account for the area difference between these two regions, however, they have seasonal magnitudes per unit area which are quite similar (4.3 compared to 4.9 cm w.e.). Thus, the offsets in 2013 and 2014 may share a common origin.

3.3. Greenland

The Greenland ice sheet has been the largest land ice contributor to sea level rise in the past decade [*Harig and Simons*, 2012; *Jacob et al.*, 2012], and its mass balance could influence the mass estimate in the nearby Canadian Archipelago, and vice versa. Mass estimation techniques vary between groups, specifically in how they compensate for signal leakage. The Slepian basis is specifically optimized to minimize leakage from the region of interest. We perform no amplitude scaling after estimating the field.

We examine the Greenland, Ellesmere, and Baffin regions separately, as well as in combination. Greenland's mass loss is roughly an order of magnitude larger than the losses from Ellesmere or Baffin (Figure 4). Since 2003 the ice sheet has lost an average of -244 ± 6 Gt/yr of ice, accelerating at a rate of -28 ± 9 Gt/yr^2.

It is notable that during 2013 Greenland experienced the same abnormally low mass loss seen in Ellesmere Island. From 2003 to 2012, the average amount of ice lost during the summer melt season (June to November) was 364 Gt, with a low of 226 Gt in 2004 and a high of 534 Gt in 2012. In contrast, during 2013 (June to November) the ice sheet lost 78 Gt. This follows 2010–2012, which were each years of record mass loss at the time. As in the case of the Canadian Archipelago we remove the long-term trend and acceleration to compare the interannual variations in mass to the average seasonal cycle (Figure 5c). The detrended data are well represented by seasonal functions prior to 2013, with variations in each year on the order of 75–125 Gt. In contrast, during 2014 the difference of the data to the seasonal cycle exceeded 500 Gt. The maximum and minimum of the average seasonal cycle in Greenland are −166 Gt and +168 Gt in each year (Table 2). Accounting for Greenland's area, this seasonal signal is 27–44% larger than in Baffin and Ellesmere Islands.

The trends from the combined regions (Table 1) are very similar to the sum of the trends from individual regions. The map patterns of ice mass loss for Greenland and Ellesmere Island are only slightly different, whether they are localized jointly or separately. This correspondence attests to the robustness of our estimates.

4. Conclusions

Mountain glaciers and ice caps remain significant contributors to sea level rise, with the Canadian Archipelago and the Gulf of Alaska experiencing large ice mass changes. Many of these glaciated regions are small, near the limit that can be resolved by GRACE data. We have analyzed time-variable gravimetry data using a spatiospectral localization technique based on spherical Slepian functions which remains very sensitive for mass estimation when the area of interest is small compared to the resolution implied by the spherical-harmonic bandwidth.

Ice mass losses continue steadily around the Gulf of Alaska with the total mass trend showing no significant acceleration. Variability in these regions is dominated by the seasonal mass cycle which is roughly 3 to 4 times as strong as the seasonal cycle around Greenland on a per square meter basis. Ice mass losses in Greenland and the Canadian Archipelago continue to accelerate over time, increasing the contribution of these areas to sea level rise. Since the summer of 2013 these regions have experienced a positive ice mass anomaly, where the yearly mass changes diverge from the long-term decadal trend. In the case of Greenland this anomaly reached nearly 500 Gt through the end of 2014. Independent verification of our findings by other, nongravimetric, studies, is underway.

Acknowledgments
Supported by the U.S. National Science Foundation, via grant NSF-1245788, by NOAA via the Princeton Cooperative Institute for Climate Science, and by the Princeton Environmental Institute. Our computer code is published, as documented by *Harig et al.* [2015].

References

Abdalati, W., W. Krabill, E. Frederick, S. Manizade, C. Martin, J. Sonntag, R. Swift, R. Thomas, J. Yungel, and R. Koerner (2004), Elevation changes of ice caps in the Canadian Arctic Archipelago, *J. Geophys. Res.*, *109*, F04007, doi:10.1029/2003JF000045.

Arendt, A. A., S. B. Luthcke, A. S. Gardner, S. O'Neel, D. Hill, G. Moholdt, and J. W. Abdalati (2013), Analysis of a GRACE global masscon solution for Gulf of Alaska glaciers, *J. Glaciol.*, *59*(217), 913–924, doi:10.3189/2013JoG12J197.

Bamber, J. L., and R. Riva (2010), The sea level fingerprint of recent ice mass fluxes, *Cryosphere*, *4*, 621–627, doi:10.5194/tc-4-621-2010.

Chen, J. L., C. R. Wilson, and B. D. Tapley (2011), Interannual variability of Greenland ice losses from satellite gravimetry, *J. Geophys. Res.*, *116*, B07406, doi:10.1029/2010JB007789.

Cheng, M., B. D. Tapley, and J. C. Ries (2013), Deceleration in the Earth's oblateness, *J. Geophys. Res. Solid Earth*, *118*, 740–747, doi:10.1002/jgrb.50058.

Flechtner, F., T. Gruber, A. Güntner, M. Mandea, M. Rothacher, T. Schöne, and J. Wickert (Eds.) (2010), *System Earth via Geodetic-Geophysical Space Techniques*, Advanced Technologies in Earth Sciences, Springer, Berlin.

Gardner, A. S., G. Moholdt, B. Wouters, G. J. Wolken, D. O. Burgess, M. J. Sharp, J. G. Cogley, C. Braun, and C. Labine (2011), Sharply increased mass loss from glaciers and ice caps in the Canadian Arctic Archipelago, *Nature*, *473*(7347), 357–360, doi:10.1038/nature10089.

Gardner, A. S., G. Moholdt, A. A. Arendt, and B. Wouters (2012), Accelerated contributions of Canada's Baffin and Bylot Island glaciers to sea level rise over the past half century, *Cryosphere*, *6*, 1103–1125, doi:10.5194/tc-6-1103-2012.

Gardner, A. S., et al. (2013), A reconciled estimate of glacier contributions to sea level rise: 2003 to 2009, *Science*, *340*(6134), 852–857, doi:10.1126/science.1234532.

Guo, J. Y., Z. W. Huang, C. K. Shum, and W. van der Wal (2012), Comparisons among contemporary glacial isostatic adjustment models, *J. Geodyn.*, *61*, 129–137, doi:10.1016/j.jog.2012.03.011.

Harig, C., and F. J. Simons (2012), Mapping Greenland's mass loss in space and time, *Proc. Natl. Acad. Sci.*, *109*(49), 19,934–19,937, doi:10.1073/pnas.1206785109.

Harig, C., and F. J. Simons (2015), Accelerated West Antarctic ice mass loss continues to outpace East Antarctic gains, *Earth Planet. Sci. Lett.*, *415*, 134–141, doi:10.1016/j.epsl.2015.01.029.

Harig, C., K. W. Lewis, A. Plattner, and F. J. Simons (2015), A suite of software analyzes data on the sphere, *Eos Trans. AGU*, *96*(6), 18–22, doi:10.1029/2015EO025851.

Jacob, T., J. Wahr, W. T. Pfeffer, and S. Swenson (2012), Recent contributions of glaciers and ice caps to sea level rise, *Nature*, *482*(7386), 514–518, doi:10.1038/nature10847.

Kennedy, R. A., and P. Sadeghi (2013), *Hilbert Space Methods in Signal Processing*, Cambridge Univ. Press, Cambridge, U. K.

King, M. A., R. J. Bingham, P. Moore, P. K. Whitehouse, M. J. Bentley, and G. A. Milne (2012), Lower satellite-gravimetry estimates of Antarctic sea-level contribution, *Nature*, *491*(7425), 586–589, doi:10.1038/nature11621.

Klees, R., E. A. Revtova, B. C. Gunter, P. Ditmar, E. Oudman, H. C. Winsemius, and H. H. G. Savenije (2008), The design of an optimal filter for monthly GRACE gravity models, *Geophys. J. Int.*, *175*, 417–432, doi:10.1111/j.1365–246X.2008.03922.x.

Little, C. M., M. Oppenheimer, and N. M. Urban (2013a), Upper bounds on twenty-first-century Antarctic ice loss assessed using a probabilistic framework, *Nat. Clim. Change*, *3*, 654–659, doi:10.1038/nclimate1845.

Little, C. M., N. M. Urban, and M. Oppenheimer (2013b), Probabilistic framework for assessing the ice sheet contribution to sea level change, *Proc. Natl. Acad. Sci.*, *110*(9), 1–6, doi:10.1073/pnas.1214457110.

Luthcke, S. B., A. A. Arendt, D. D. Rowlands, J. J. McCarthy, and C. F. Larsen (2008), Recent glacier mass changes in the Gulf of Alaska region from GRACE mascon solutions, *J. Glaciol.*, *54*(188), 767–777, doi:10.3189/002214308787779933.

Luthcke, S. B., T. J. Sabaka, B. D. Loomis, A. A. Arendt, J. J. McCarthy, and J. Camp (2013), Antarctica, Greenland and Gulf of Alaska land-ice evolution from an iterated GRACE global mascon solution, *J. Glaciol.*, *59*(216), 613–631, doi:10.3189/2013JoG12J147.

Paulson, A., S. Zhong, and J. Wahr (2007), Inference of mantle viscosity from GRACE and relative sea level data, *Geophys. J. Int.*, *171*(2), 497–508, doi:10.1111/j.1365–246X.2007.03556.x.

Pfeffer, W. T., et al. (2014), The Randolph Glacier Inventory: A globally complete inventory of glaciers, *J. Glaciol.*, *60*(221), 537–551, doi:10.3189/2014JoG13J176.

Plattner, A., and F. J. Simons (2015), Potential-field estimation using scalar and vector Slepian functions at satellite altitude, in *Handbook of Geomathematics*, edited by W. Freeden, M. Z. Nashed, and T. Sonar, 2nd ed., pp. 2003–2055, Springer, Heidelberg, Germany, doi:10.1007/978-3-642-54551-1_64.

Reager, J. T., A. S. Gardner, J. S. Famiglietti, D. N. Wiese, A. Eicker, and M.-H. Lo (2016), A decade of sea level rise slowed by climate-driven hydrology, *Science*, *351*(6274), 699–703, doi:10.1126/science.aad8386.

Rowlands, D. D., S. B. Luthcke, S. M. Klosko, F. G. R. Lemoine, D. S. Chinn, J. J. McCarthy, C. M. Cox, and O. B. Anderson (2005), Resolving mass flux at high spatial and temporal resolution using GRACE intersatellite measurements, *Geophys. Res. Lett.*, *32*, L04310, doi:10.1029/2004GL021908.

Sasgen, I., M. van den Broeke, J. L. Bamber, E. Rignot, L. S. Sørensen, B. Wouters, Z. Martinec, I. Velicogna, and S. B. Simonsen (2012), Timing and origin of recent regional ice-mass loss in Greenland, *Earth Planet. Sci. Lett.*, *333–334*, 293–303, doi:10.1016/j.epsl.2012.03.033.

Schrama, E. J. O., B. Wouters, and D. A. Lavallée (2007), Signal and noise in Gravity Recovery and Climate Experiment (GRACE) observed surface mass variations, *J. Geophys. Res.*, *112*, B08407, doi:10.1029/2006JB004882.

Shepherd, A., et al. (2012), A reconciled estimate of ice-sheet mass balance, *Science*, *338*(6111), 1183–1189, doi:10.1126/science.1228102.

Simons, F. J., and F. A. Dahlen (2006), Spherical Slepian functions and the polar gap in geodesy, *Geophys. J. Int.*, *166*(3), 1039–1061, doi:10.1111/j.1365-246X.2006.03065.x.

Simons, F. J., and A. Plattner (2015), Scalar and vector Slepian functions, spherical signal estimation and spectral analysis, in *Handbook of Geomathematics*, edited by W. Freeden, M. Z. Nashed, and T. Sonar, 2nd ed., pp. 2563–2608, Springer, Heidelberg, Germany, doi:10.1007/978-3-642-54551-1_30.

Simons, F. J., F. A. Dahlen, and M. A. Wieczorek (2006), Spatiospectral concentration on a sphere, *SIAM Rev.*, *48*(3), 504–536, doi:10.1137/S0036144504445765.

Slepian, D. (1983), Some comments on Fourier analysis, uncertainty and modeling, *SIAM Rev.*, *25*(3), 379–393.

Sterenborg, M. G., E. Morrow, and J. X. Mitrovica (2013), Bias in GRACE estimates of ice mass change due to accompanying sea-level change, *J. Geod.*, *87*(4), 387–392, doi:10.1007/s00190-012-0608-x.

Stocker, T. F., D. Qin, G.-K. Plattner, M. Tignor, S. K. Allen, J. Boschung, A. Nauels, Y. Xia, V. Bex, and P. M. Midgley (Eds.) (2013), Climate change 2013: The physical science basis. Contribution of working group I to the fifth assessment report, *Tech. Rep.*, Intergovernmental Panel on Climate Change, Cambridge, U. K.

Swenson, S., J. M. Wahr, and P. C. D. Milly (2003), Estimated accuracies of regional water storage variations inferred from the Gravity Recovery and Climate Experiment (GRACE), *Water Resour. Res.*, *39*(8), 1223, doi:10.1029/2002WR001808.

Swenson, S., D. Chambers, and J. Wahr (2008), Estimating geocenter variations from a combination of GRACE and ocean model output, *J. Geophys. Res.*, *113*, B08410, doi:10.1029/2007JB005338.

Tapley, B. D., S. Bettadpur, J. C. Ries, P. F. Thompson, and M. M. Watkins (2004), GRACE measurements of mass variability in the Earth system, *Science*, *305*(5683), 503–505, doi:10.1126/science.1099192.

Velicogna, I. (2009), Increasing rates of ice mass loss from the Greenland and Antarctic ice sheets revealed by GRACE, *Geophys. Res. Lett.*, *36*, L19503, doi:10.1029/2009GL040222.

Velicogna, I., and J. Wahr (2013), Time-variable gravity observations of ice sheet mass balance: Precision and limitations of the GRACE satellite data, *Geophys. Res. Lett.*, *40*, 3055–3063, doi:10.1002/grl.50527.

Velicogna, I., and J. M. Wahr (2006), Acceleration of Greenland ice mass loss in spring 2004, *Nature*, *443*, 329–331, doi:10.1038/nature.05168.

Wahr, J. M., M. Molenaar, and F. Bryan (1998), Time variability of the Earth's gravity field: Hydrological and oceanic effects and their possible detection using GRACE, *J. Geophys. Res.*, *103*(B12), 30,205–30,229, doi:10.1029/98JB02844.

Wahr, J. M., S. Swenson, and I. Velicogna (2006), Accuracy of GRACE mass estimates, *Geophys. Res. Lett.*, *33*, L06401, doi:10.1029/2005GL025305.

Williams, S. D. P., P. Moore, M. A. King, and P. L. Whitehouse (2014), Revisiting GRACE Antarctic ice mass trends and accelerations considering autocorrelation, *Earth Planet. Sci. Lett.*, *385*, 12–21, doi:10.1016/j.epsl.2013.10.016.

Wouters, B., J. L. Bamber, M. R. van den Broeke, J. T. M. Lenaerts, and I. Sasgen (2013), Limits in detecting acceleration of ice sheet mass loss due to climate variability, *Nat. Geosci.*, *6*(8), 613–616, doi:10.1038/ngeo1874.